Dynamics of Alpha Control: Preparatory Suppression of Posterior Alpha Oscillations by Frontal Modulators Revealed with Combined EEG and Event-related Optical Signal

Kyle E. Mathewson[1], Diane M. Beck[1], Tony Ro[2], Edward L. Maclin[1], Kathy A. Low[1], Monica Fabiani[1], and Gabriele Gratton[1]

Abstract

■ We investigated the dynamics of brain processes facilitating conscious experience of external stimuli. Previously, we proposed that alpha (8–12 Hz) oscillations, which fluctuate with both sustained and directed attention, represent a pulsed inhibition of ongoing sensory brain activity. Here we tested the prediction that inhibitory alpha oscillations in visual cortex are modulated by top–down signals from frontoparietal attention networks. We measured modulations in phase-coherent alpha oscillations from superficial frontal, parietal, and occipital cortices using the event-related optical signal (EROS), a measure of neuronal activity affording high spatiotemporal resolution, along with concurrently recorded EEG, while participants performed a visual target detection task. The pretarget alpha oscillations measured with EEG and EROS from posterior areas were larger for subsequently undetected targets, supporting alpha's inhibitory role. Using EROS, we localized brain correlates of these awareness-related alpha oscillations measured at the scalp to the cuneus and precuneus. Crucially, EROS alpha suppression correlated with posterior EEG alpha power across participants. Sorting the EROS data based on EEG alpha power quartiles to investigate alpha modulators revealed that suppression of posterior alpha was preceded by increased activity in regions of the dorsal attention network and decreased activity in regions of the cingulo-opercular network. Cross-correlations revealed the temporal dynamics of activity within these preparatory networks before posterior alpha modulation. The novel combination of EEG and EROS afforded localization of the sources and correlates of alpha oscillations and their temporal relationships, supporting our proposal that top–down control from attention networks modulates both posterior alpha and awareness of visual stimuli. ■

INTRODUCTION

A long tradition considers 8–12 Hz alpha oscillations in the EEG as indexing reduced excitation (Lopes Da Silva, 1991; Berger, 1929). Recent research has pointed to alpha as a control mechanism for implementing specific, dynamic interactions between cortical processes. Klimesch (1999) proposed that suppression of alpha after task-relevant stimuli indicates decreased inhibition in task-processing areas. This framework has developed into several theories suggesting that alpha oscillations reflect a neural mechanism to spatially and temporally select or suppress information (Mathewson et al., 2011, 2012; Jensen & Mazaheri, 2010; Mathewson, Gratton, Fabiani, Beck, & Ro, 2009; Klimesch, Sauseng, & Hanslmayr, 2007). Inhibitory alpha activity commonly observed in sensory and motor regions (Jensen & Mazaheri, 2010) should be modulated by cortical areas involved in top–down attention control, according to these proposals.

Consistent with our proposal, evidence suggests that activity in distinct frontoparietal networks associated with sustained and directed attention correlates with fluctuations in posterior alpha amplitude. Hemodynamic activity in the dorsal attention network (DAN; Corbetta & Shulman, 2002) is negatively correlated with EEG alpha power (Sadaghiani et al., 2010; Laufs et al., 2003), whereas regions of the default mode network (DMN; Mo, Liu, Huang, & Ding, 2012; Ben-Simon, Podlipsky, Arieli, Zhdanov, & Hendler, 2008) and cingulo-opercular network (CON; Sadaghiani et al., 2010, 2012; Dosenbach et al., 2007; Laufs et al., 2003) have shown the opposite relationship. Correspondingly, repetitive TMS of DAN's right inferior parietal sulcus (IPS) or right FEFs suppresses both posterior alpha desynchronization and the detection advantages normally accompanying shifts of spatial attention (Capotosto, Babiloni, Romani, & Corbetta, 2012; Hamidi, Slagter, Tononi, & Postle, 2009).

Here we investigated how top–down control from frontoparietal networks influences alpha modulations in visual cortex and, in turn, fluctuations in visual awareness. We concurrently recorded fast optical imaging

[1]University of Illinois at Urbana-Champaign, [2]The City College of the City University of New York

Journal of Cognitive Neuroscience 26:10, pp. 2400–2415
doi:10.1162/jocn_a_00637

(the event-related optical signal [EROS]; Gratton & Fabiani, 2010; Gratton et al., 1995a) and EEG data while participants performed a metacontrast masking task (Mathewson et al., 2009). The high spatial and temporal resolution of EROS afford the unique opportunity not only of correlating EROS frontoparietal activity with EEG alpha power but also of searching for areas that are themselves oscillating in the alpha range in the optical data.

Fast optical imaging involves shining near-infrared light into the head to measure changes in the brain's intrinsic light scattering properties, which have been shown to coincide with electrical activity (Rector, Carter, Volegov, & George, 2005; Rector, Poe, Kristensen, & Harper, 1997; Cohen, 1973; Hill & Keynes, 1949). Light diffusion through the brain is modified by local brain activity. Along with the aggregated ionic transfer associated with neuronal depolarization and axonal firing, osmotic pressure leads to a net influx of extracellular water into the cell (Witte, Niermann, & Holthoff, 2001). This influx stretches the flexible membrane of the cell (Momose-Sato, Sato, Hirota, & Kamino, 1998; Sato, Momose-Sato, Arai, Hirota, & Kamino, 1997), allowing photons traversing a large activated area to be relatively less impeded and thus travel further (Syková, Kubinová, Jendelová, & Chvátal, 2003). The additional distance traveled from light source to detector in the more transparent (less scattering) tissue leads to picosecond-range delays in the time of flight of photons traversing active brain tissue compared with inactive tissue (Lee & Kim, 2010), providing a noninvasive and spatiotemporally precise window into neural activity (Rector et al., 2005; Andrew & MacVicar, 1994).

Noninvasive fast optical imaging signals in humans are analogous to the well-studied intrinsic scattering signals measured in vivo in single neurons, exposed cortex (Frostig & Chen-Bee, 2009), and intracranial recordings (Rector et al., 1997, 2005). Fast optical signals can be distinguished from hemodynamic and metabolic optical changes based on their lack of spectral specificity and on their much faster time course than major hemodynamic responses (Fabiani et al., 2014; Franceschini & Boas, 2004; Gratton, Goodman-Wood, & Fabiani, 2001). Changes in light due to movement and other nonneuronal tissue in the scalp, muscles, and skin have also been ruled out, and the distribution of signal to noise across the cortex is generally uniform (e.g., Parks et al., 2012; Gratton & Fabiani, 2010; Medvedev, Kainerstorfer, Borisov, Gandjbakhche, & VanMeter, 2010). EROS has been used in our lab and others to image neural activity in a large number of visual and attention tasks (Chiarelli, DiVacri, Romani, & Merla, 2012; Tse, Gordon, Fabiani, & Gratton, 2010; Medvedev, Kainerstorfer, Borisov, Barbour, & VanMeter, 2008; Zhang et al., 2007; Gratton & Fabiani, 2003; Gratton et al., 1997, 2001; Gratton, Sarno, Maclin, Corballis, & Fabiani, 2000; see Gratton & Fabiani, 2010, for an in depth review). Several papers have reported a strong correspondence between fast optical and ERP responses (e.g., Fabiani et al., 2014; Sun, Zhang, Gong, Sun, & Luo, 2014; Huang, Wang, Jia, Mo, & Chen, 2013; Medvedev et al., 2010; Tse et al., 2007). Importantly, Tse and colleagues (2010) demonstrated the feasibility of measuring oscillatory alpha activity using EROS by finding frequency domain EROS steady-state responses to visual stimulation at various frequencies.

By measuring the temporal delay of modulated light diffusing through the cortex to nearby detectors, EROS provides a unique noninvasive, spatiotemporally precise window onto brain activity, making it ideally suited for pinpointing underlying generators of EEG oscillations. Here, we used a novel combination of concurrent EEG and EROS recording to localize the source of the posterior alpha suppression associated with enhanced detection and to identify potential top–down modulators of the alpha power changes as well as the temporal dynamics among these areas.

Specifically, we first sought to replicate the findings of Mathewson et al. (2009) showing that decreased EEG alpha power precedes detected (compared with undetected) targets. Second, we compared alpha frequency EROS activity preceding detected and undetected targets to determine which cortical regions may be the source of these oscillatory modulations. Third, using EEG alpha power to sort the EROS data into bins, we examined the relationship between frontal cortical regions and variations in EEG alpha power. Finally, cross-correlation analyses of the broadband EROS data were used to determine the sequence of cortical activations leading to changes in posterior alpha activity.

To preview the results, we localized the major prestimulus alpha modulations relevant for subsequent visual target detection to the cuneus and precuneus regions and identified the frontal and parietal modulators of this preparatory activity. We thereby illuminate the top–down control of preparatory oscillatory modulation of sensory activity and the influence of these oscillations on subsequent visual awareness using a novel combination of EEG and EROS.

METHODS

Participants

Sixteen paid participants (nine women; age range = 19–29 years) were recruited from the university community and gave informed consent as approved by the Institutional Review Board of the University of Illinois. Each participant completed two experimental sessions in which both EROS and EEG were recorded from a montage covering most of superficial occipital, parietal, and frontal cortices. A T1-weighted volumetric structural MRI (3T Siemens Allegra scanner, MPRAGE sequence) and 3-D digitization of the source and detector locations on the head, fiducial landmarks, and ~250 additional scalp locations were obtained from each participant and used to

coregister the optical data onto each individual's cortical anatomy (Whalen, Maclin, Fabiani, & Gratton, 2008).

Metacontrast Masking Task

Participants performed two metacontrast masking sessions on different days. Each session consisted of 16 blocks of 72 trials, for a total of 2304 trials per participant over both EEG/EROS recording sessions. The stimuli and trial timeline are shown in Figure 1. Each 2248.9-msec trial began with a 247-msec warning stimulus (a fixation cross), followed by a 400-msec blank screen. A constant interval was used between the warning and the target stimulus to maximize the phase- and time-locking of preparatory alpha activity. A 1° circular target was then presented at fixation for 11.7 msec (one refresh cycle of the 85-Hz Sony Trinitron cathode ray tube monitor), at a fixed viewing distance of 57 cm. The target was followed, after a 46.8-msec blank ISI, by a 23.4-msec metacontrast annulus mask with a 2° outer diameter and 1° aperture. The fixation cross was black, and the target and mask were dark gray, all presented on a light gray background. The contrast, luminance, and duration of the stimuli were determined on the basis of pilot studies (Mathewson et al., 2009, 2012), showing that this combination of parameters resulted in target detection rates in the range of 50%.

Finally, participants indicated, within 1520 msec via an E-prime button box, whether they had (Button 1) or had not (Button 5) detected the target. On a random 25% of the trials, the target was omitted to measure false alarms, and on 25% of the trials, the target was presented with no mask. Only the masked target trials (1152 per participant) are considered here. Participants were instructed to sit still, relax, and fixate the central fixation cross. All participants performed at least one block of practice trials before the experimental manipulation to familiarize themselves with the task.

EEG

EEG Recording and Preprocessing

We measured the EEG from eight customized Ag/AgCl electrodes. The electrodes were placed at the end of 6-cm plastic tubes filled with conductive gel and positioned such that the conductive area of the electrode was flush with the bottom of the tube. These tubes were inserted and secured into specific holes in the same helmet that held the optical sources and detectors. The electrode locations were close to F3, F4, P3, P4, T5, T6, O1, and O2 in the 10/20 system and were in the same positions across recording sessions and participants. Electrodes were referenced to the left mastoid online and to an arithmetically derived average mastoid offline with a forehead ground. Bipolar electrode pairs above and below the right eye and slightly lateral from the outer canthus of each eye recorded the vertical and horizontal EOG, respectively. Data were recorded at 100 Hz with a 0.01–30 Hz half-amplitude band-pass filter. Electrode impedance was kept below 20 kΩ. Offline, data were epoched into 2200-msec segments (−847 to 1353 msec; 0 msec = Target onset). First, prefixation baseline-subtracted epochs with an absolute voltage exceeding 1000 μV were discarded to remove trials with digitizer saturation or physical electrode displacements. Next, the variance in the EEG channels accounted for by eye movements on the EOG channels was removed using a regression technique described in Gratton, Coles, and Donchin (1983). Finally, trials with voltage fluctuations

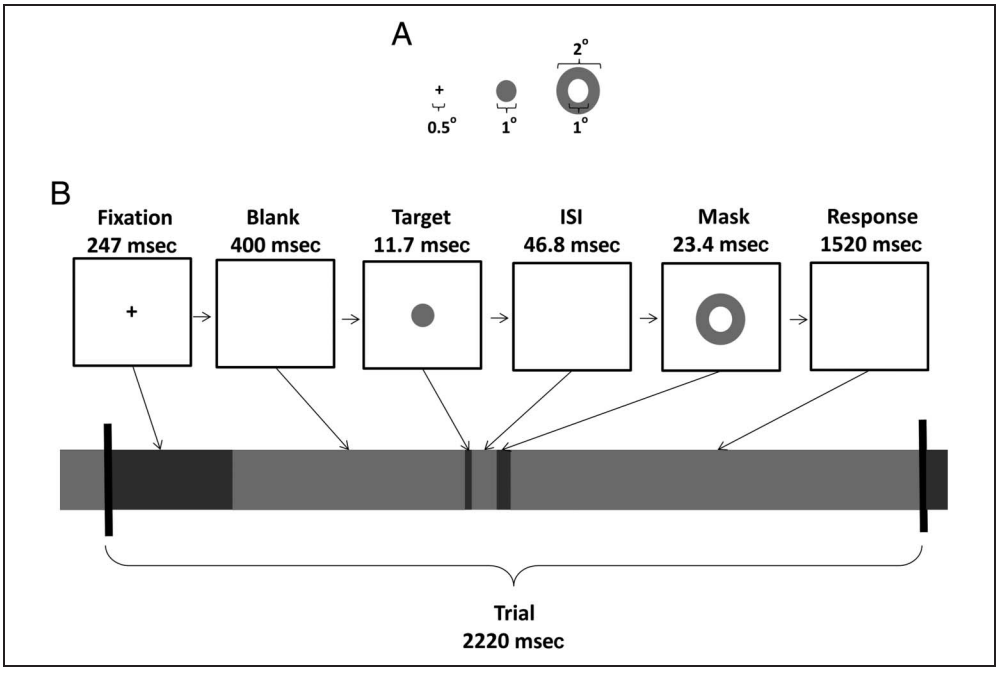

Figure 1. Stimulus dimensions (A) and trial timeline (B).

Table 1. Summary of Analyses

Data	*Analysis*	*Figures*
Single Trial EEG (O1 and O2; 0.01–30 Hz)	• Baseline subtracted ERSP	3
	• 8–12 Hz window, 647 msec pretarget	
Trial average EROS (0.1–15 Hz)	• Baseline subtracted EROS	4–5
	• Phase-locked 9.8 Hz alpha power	
Single trial EEG alpha (O1 and O2; −400 to 200 msec; 8–12 Hz)	• EEG power quartiles	6
	• EROS averages based on EEG quartiles	
Single trial EROS (39.1 Hz; 0.1–15 Hz)	• Voxel-level summed, weighted average showing linear relationships	
EROS cuneus alpha difference (9.8 Hz; detected − undetected)	• Backward cross-correlations	7B
Trial average EROS full brain (0.1–15 Hz; detected − undetected)	• 30 pretarget time points	
	• Seed: Cuneus peak alpha difference	
	• Correlate: full brain broadband difference	

ERSP = event-related spectral perturbation; EEG = electroencephalogram; EROS = event-related optical signal.

having an absolute value greater than 500 μV after eye movement correction were removed to minimize the influence of any remaining artifactual activity. Because of the higher impedance values necessary to facilitate concurrent EEG and EROS recording, these artifact thresholds were created to be somewhat lenient so as to retain the maximal number of simultaneously recorded EEG and EROS trials. On average, 7.5% of trials per participant were removed (median = 2.3%), with no difference in the removal of undetected (M = 7.6%) and detected target trials (M = 7.1%; $t(15) = 0.68$; *ns*). Use of stricter thresholds did not significantly change the EEG results.

EEG Time–Frequency Analysis

A summary of the analyses described in this and the following sections is presented in Table 1. Moving window fast Fourier transforms (FFTs) were applied on the 2200-msec trial epochs. Hamming windowed segments of data were 640 msec long and were zero-padded with a ratio of 2 to create 128 data points for each FFT, with successive FFT windows overlapping by 98.2%. The FFTs provided estimates of spectral power between 0.78 and 30 Hz, every 0.78 Hz and every 11.77 msec. We employed an event-related spectral perturbation technique. On each trial, the average spectrum over the 200-msec prefixation period was subtracted from the rest of the epoch to eliminate the differences in baseline spectra between participants, and over time within participants, and to visualize the variations in oscillatory activity developing throughout the trial. We were specifically interested in the power of alpha activity before the onset of the target, which we have previously found to be larger preceding subsequently undetected than detected targets (Mathewson et al., 2009). We therefore restricted our statistical analysis to the average activity between 8 and 12 Hz during the 647-msec fixation and blank screen periods directly preceding the onset of the target, pooling over posterior O1 and O2 electrodes to minimize noise. Data from the end of this window were excluded because some evoked activity from the target stimulus is present in the later time periods.

EROS

Optical Recording

We measured scattering changes of near-infrared light using six synchronized frequency-domain oximeters (Imagent; ISS, Inc., Champaign, IL), each with four detectors, for a total of 24 detectors. Near-infrared light from a total of 64 laser diode sources (830 nm) was carried to the scalp by 400 μm silica optic fibers in plastic sheathing. The 24 photomultiplier tube detectors collected light from each nearby source through separate 3-mm diameter fiber-optic bundles that were held flush against the scalp, with the hair moved aside (Figure 2A). The laser diodes were amplitude-modulated at a rate of 110 MHz, and the gain of the detectors was modulated at 110.003125 MHz, creating a heterodyne beat frequency in the transduced output of the detectors at 3.125 kHz. The electrical output of the photomultiplier detectors was band-pass filtered at 3.125 kHz, digitized at a rate of 50 kHz, and FFTs of 1.28-msec segments of the resultant data were computed, with the phase of the 3.125 kHz difference providing relative measurements of the modulated light's delay in degrees. The resultant photon delay signal was then converted into picoseconds.

Source and detector fibers were held in position against the scalp by a modified, fitted, motorcycle helmet with securing adapters (Figure 2A). Care was taken to prevent any environmental or stimulus light from entering the enclosed helmet. To increase spatial sampling resolution, the montage of source and detector locations was shifted to the left or right by ~2 cm across the two experimental sessions, with the order counterbalanced across participants. The locations of the 128 source and 48 detector fibers across the two sessions, as well as the ~250 additional scalp points used for MRI coregistration, are shown in Figure 2B and C, coregistered onto a scalp reconstruction from the structural MRI of the same participant. Locations were spread out maximally over the two recording sessions to cover as much of the cortex as possible, thereby achieving an optimal density of recording and maximizing the number of channels with source detector distances between 1.5 and 6.0 cm. Shorter source detector channel distances detect light that has not reached the cortex, whereas longer channel distances receive insufficient light for a reliable signal (Gratton et al., 2000). Given the probabilistic 3-D reconstruction of the photon path described in more detail below, these distances provide recording depths up to 3 cm from the scalp (Figure 2D).

To rule out any cross-talk between a pair of coilluminated laser sources whose light reached the same detector, only four light sources were on at any given time, and of the four light sources illuminated during any multiplex cycle, only one was within 6 cm of any given detector. Given the large number of sources and detectors, we developed an algorithm (NOMAD, Near-infrared Optode Montage Automated Design; www.kylemathewson.com/optical) inspired by graph-coloring theory to assign and constrain specific sources to particular intervals within the multiplexing cycle. Thus, each of the 24 detectors was illuminated by 16 multiplexed light sources providing 384 channels per session. The resulting sampling rate for whole-brain imaging was approximately 39.1 Hz, providing a cortical image every 25.6 msec.

EROS Preprocessing and 3-D Reconstruction

EROS is derived from the continuous fast optical signal by creating a stimulus-locked average over many identical trials, thereby increasing the ratio of the time-locked

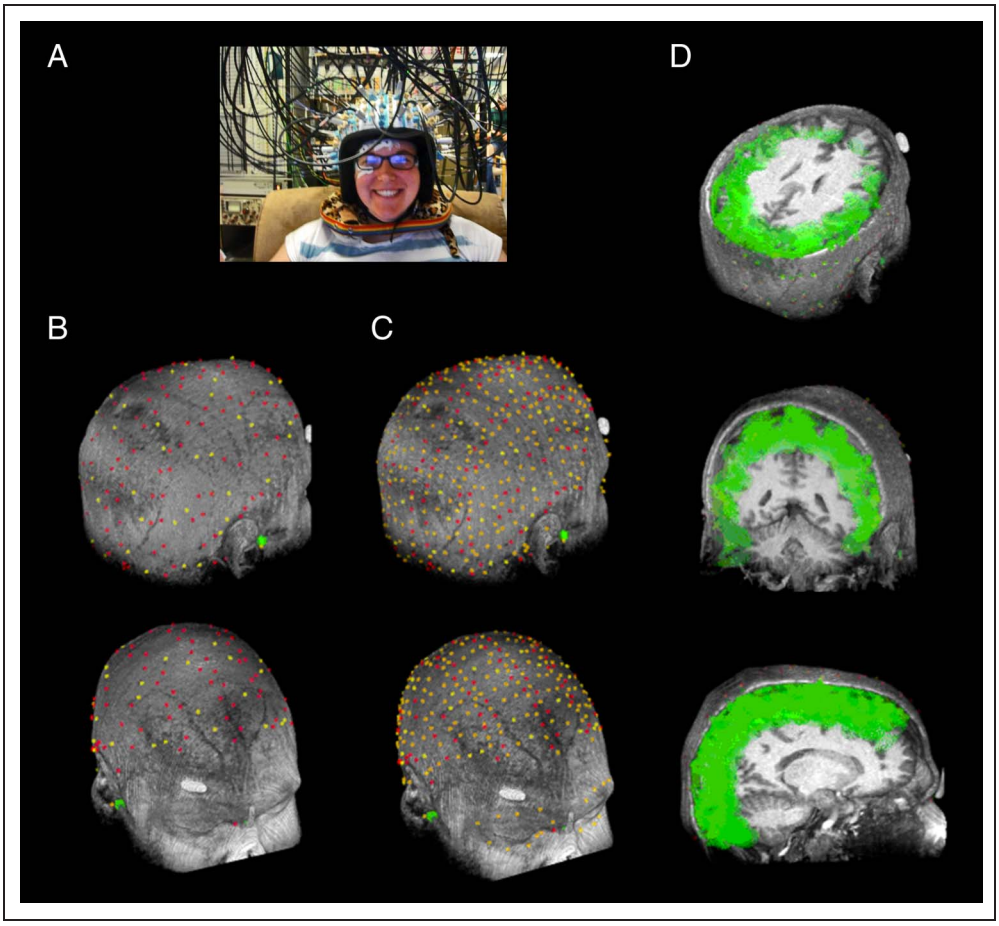

Figure 2. (A) Image of the experimental setup showing the EROS equipment, with source and detector fibers traveling to and from the head attached with a modified motorcycle helmet. Electrodes for adjacent EEG equipment are attached to the skin or placed in tubes that also fit inside the helmet and are positioned against the head. (B) Position of each of the sources (red) and detectors (yellow) across both sessions, coregistered with the individual's structural MRI for a representative participant. (C) In addition to the 128 sources and 48 detectors, the locations of an additional ~250 points (also red and yellow), including nasion and preauricular common fiducial landmarks (green dots) on the scalp and face, were used to enhance the coregistration process. (D) Three-dimensional reconstruction of the estimated light path of each optical channel between a source and detector in A are shown as green ellipsoids for each channel, again overlaid on the structural MRI of the same participant from three oblique angles. Note the consistent and widespread coverage of the cortical surface by the optical imaging montage and the depth of coverage up to ~30 mm from the scalp.

signal to the randomly timed and phased noise. Data from the 768 recording channels were preprocessed using P-POD (Pre-Processing of Optical Data, MATLAB code). Channels with a source detector distance greater than 6.0 cm were removed from further processing. Channels with a standard deviation of the photon delay greater than 160 psec were removed to limit the influence of noise. The photon delay data were then corrected for phase-wrapping of the otherwise noncontiguous circular optical phase delay signal, normalized, and detrended to remove low-frequency drifts (<~.005 Hz) using a third-order polynomial. Next, the pulse signal was removed from all data segments using a time-warping regression procedure (Gratton & Corballis, 1995). The data were then filtered (0.1–15 Hz half-amplitude pass band) to remove any remaining hemodynamic activity, signals due to nonbiological processes, and other biological noise. Next, 2200-msec segments of these continuous data, locked to the onset of each target (−847 to 1353 msec) were selected and averaged over trials, separately for each condition (i.e., detected vs. undetected) providing event-related averages of the brain activity for each source detector pair in the same time period as the EEG data. This trial averaging allowed us to isolate alpha modulation in the pretarget interval that was phase-locked with the warning cue across trials.

The 3-D location of each source and detector was obtained with a Polhemus "3Space" Fasttrak 3D digitizer (Colchester, VT) with an extended stylus, and Locator 4.1 software (Source Signal Imaging, Inc., San Diego, CA). These locations (Figure 2B) as well as an oversampled collection of additional scalp and face locations (Figure 2C) were coregistered onto a scalp model reconstructed from the T1 weighted volumetric structural MRI of each participant, first, by coregistering common fiducial landmarks (nasion and preauricular points) and then by using least square fitting procedures to adjust the fit to minimize errors below 5 mm (Whalen et al., 2008). The coregistered brain locations were then transformed into common Talairach coordinates for group level analysis.

Next, in-house software Opt-3D was used to reconstruct in voxel space the resultant light diffusion path, which was modeled as a curved ellipsoid of fixed size based on the source detector distance (Gratton, 2000). The measured delays in light because of neuronal scattering are also a result of changes in the path of light, but these changes are three orders of magnitude smaller than those caused by differences in channel distance, so are inconsequential to the 3-D reconstruction. The average photon delay signal from each channel was thus attributed uniformly to the 3-D volume of the light's path. Voxels of the brain with two or more estimated overlapping light paths were assigned an average of those channels. Most voxels had between 5 and 10 overlapping channels for each participant. After reconstruction, all nonbrain voxels were masked from analysis and visualization.

Modeled representations of the volumes sampled by all recording channels between 1.5 and 6.0 cm apart are presented for a single representative participant over the coregistered MRI data in Figure 2D, sliced to reveal the coverage from each of the three Talairach directions, indicating the broad and consistent coverage provided by the full-head optical montages. Further indication of the broad coverage we achieved can be seen in the EROS data images (see Figures 5B and 6C), where dark gray areas represent the voxels sampled by at least one channel across a sufficient number ($N > 4$) of participants to satisfy the assumptions and robustness of the statistical tests described below. The resultant voxel data were then either shown as sagittal slices or orthogonally projected onto templates of the superior axial and posterior coronal surfaces of the brain. Only data superior and posterior to the anterior commissure were projected onto the axial and coronal surfaces, respectively, whereas the sagittal slices represent only voxels from that slice. Each of these statistically thresholded projections and slices are displayed uncorrected for multiple comparisons, as is typical in the initial presentation of fMRI data. Whereas more conservative corrections are used for our ROI analyses of predicted areas, this more liberal first pass allows for the visualization of the full extent of any relationships with alpha that might exist.

For statistical testing, an ROI analysis was employed, controlling for multiple comparisons using random field theory techniques applied to statistical parametric mapping, commonly used in neuroimaging analysis (Kiebel, Poline, Friston, Holmes, & Worsley, 1999; Worsley & Friston, 1995). Cubic ROIs were created around peak values derived from the literature and projected onto the relevant 2-D images for pixel-based analysis. Different sets of ROIs were used depending on the focus of the analysis, as described below. The label, coordinates, and justification for each ROI are reported in Table 2. Successive time points were tested independently. To increase statistical power, data were spatially smoothed with an 8-mm FWHM Gaussian spatial filter. Both this spatial smoothing and the temporal filtering of the signal in the frequency domain led to high multicollinearity in the voxels over time and space, further minimizing the influence of the multiple comparisons on the chance of finding false positives. For example in a grand-averaged surface projection of the difference between detected and undetected trials, there is a high correlation between two successive time points (average $r = .35$) and between two adjacent voxels ($r = .93$).

To make statistical inferences about the EROS activity at each pixel within a 2-D ROI projection, we computed a t statistic at the group level with an error term pooled over time for each relevant contrast described below. Those t statistics were then converted to z scores to control for differences in the degrees of freedom of individual voxels because of different numbers of participants contributing data to some voxels. Note that this technique is more conservative for voxels with lower

Table 2. Talairach Coordinates of ROIs

ROI	x_L, x_R/y_P, y_A/z_I, z_S	*References*
Dorsal Attention Network (DAN)		
rSFG/MFG	20, 50/5, 45/10, 40	Low et al., 2006, 2009; He et al., 2002
rTPJ/IPS	30, 60/−90, −50/0, 30	Sadaghiani et al., 2010; Copotosto et al., 2009; Hamidi et al., 2009; Moosmann et al., 2003; He et al., 2002; Laufs et al., 2002
lTPJ/IPS	−30, −60/−90, −50/0, 30	Sadaghiani et al., 2010; Laufs et al., 2003; Moosmann et al., 2003
Cuneus/precuneus	−20, 20/−100, −70/15, 45	Moosmann et al., 2003; Talairach & Tournoux, 1988
lSFG/MFG	−20, −50/5, 45/10, 40	Low et al., 2006, 2009
rFEF	25, 45/−10, 10/40, 60	Copotosto et al., 2009; Hamidi et al., 2009; He et al., 2002
Cingulo-opercular Network (CON)		
dACC/medial pFC	−20, 20/20, 50/25, 45	Sadaghiani et al., 2010; Laufs et al., 2003; Talairach & Tournoux, 1988
rAnterior pFC	25, 45/30, 50/10, 30	Sadaghiani et al., 2010

ROIs were constructed to incorporate peak activations from the listed references; x, y, z are Talairach coordinates; L/R = left/right; P/A = posterior/anterior; I/S = inferior/superior; r/l = right/left hemisphere.

statistical power. The points of peak EROS activation, the original t scores, the z scores, and the adjusted critical z value necessary for rejecting the null hypothesis (no effect) at $p < .05$ are reported below. Except where indicated below, all predicted differences were directional so one-tailed tests were used. Each ROI was analyzed independently.

EROS Time–Frequency Analysis

We used a time–frequency analysis of the stimulus-averaged EROS activity to estimate the power of alpha activity phase-locked to the onset of an incoming target. This time–frequency analysis was carried out separately for each location and for detected and undetected targets, generating a reconstruction of the time course of coherent alpha power that differed as a function of target detection. We took the trial-averaged EROS photon delays for each channel over time and submitted them to a FFT with a 205-msec moving window and with a zero-pad ratio of 2, providing estimates of spectral power (in picoseconds^2 units) every 2.4 Hz. We considered the activity over time in the bin centered at 9.8 Hz, closest to the center of the alpha frequency range. These alpha power envelopes based on the EROS averages were computed for each optical channel in each participant and condition and were then 3-D reconstructed. Because past research has shown strong negative correlations between alpha power and activity in the DAN, ROIs were constructed around the frontal and parietal areas associated with task preparation in prior EROS studies (Low, Leaver, Kramer, Fabiani, & Gratton, 2006, 2009) and DAN areas shown to be associated with modulations in alpha power (He et al., 2007; Corbetta & Shulman, 2002) including the superior and middle frontal gyri, the inferior parietal lobes and temporal-parietal junction, and the cuneus (Sadaghiani et al., 2010; Moosmann et al., 2003; Laufs et al., 2002; Table 2). The peak differences in alpha power between detected and undetected targets in each ROI were compared over participants. For brain areas in the DAN, we hypothesized that phase-locked alpha oscillations before detected targets should be reduced in power relative to undetected targets justifying the use of a one-tailed test.

Sorting EROS by EEG Alpha Power

In addition to identifying areas whose activity is modulated in the alpha-frequency range, we also sought to find control areas that modulate alpha activity, though not themselves oscillating at 8–12 Hz. Recording errors prohibited matching the EROS and EEG trials for four participants who were excluded from this analysis, leaving only 12 participants' data available.

For this analysis, we measured the evoked alpha (8–12 Hz) power on each trial from 400 to 200 msec before the onset of the target, averaged across the O1 and O2 electrodes (where and when the EEG and EROS alpha power differences were maximal; Figures 3 and 5). We divided each participant's trials into four quartiles of pretarget alpha power and then rearranged each participant's single-channel EROS trials into four separate averages based on these alpha power quartiles measured

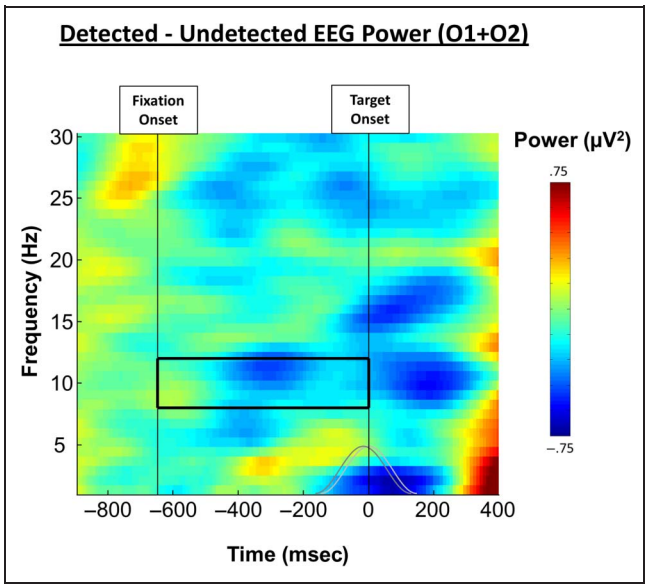

Figure 3. EEG alpha. The event-related spectral power for detected targets subtracted from that for undetected targets revealed a significant difference in 8–12 Hz EEG alpha oscillations from between 200 and 400 msec before the onset of the target. Shown is this difference over frequency and time, averaged together from the two occipital electrodes (O1 and O2). The gray lines represent the size, shape, and overlap of the moving Hamming window FFT used to compute the data and the solid box represents the 8–12 Hz window of interest used for analysis.

with EEG, ignoring detection. We then reconstructed the data in 3-D and projected them onto the relevant 2-D images as in the previous analyses. A linear trend contrast for each participant across the four alpha amplitude bins was used to identify voxels whose broadband (0.1–15 Hz) EROS activity monotonically increased or decreased as a function of the EEG alpha power. This was achieved by multiplying each average by one of four linearly increasing and zero-centered weights (−1.5, −0.5, 0.5, 1.5). The results of this linear trend weighting on EROS activation were then averaged over the entire pretarget period (mean amplitude from −650 to 0 msec), providing a single brain image of the extent to which EROS activity monotonically increased or decreased with simultaneous EEG alpha power. This amounts to a type of rank-order correlation between EROS activity and EEG alpha power. This value was positive if EROS alpha activity increased across the four EEG alpha power bins. Images were then combined across participants as a t test of this weighted average against the null hypothesis of no linear relationship between EROS activity and EEG alpha power quartile. These data identify areas that are possible candidate modulators of posterior alpha activity.

We used three different frontal ROIs for the statistical analysis of these candidate modulators (see Table 2). These ROIs include a frontal area of the DAN, the FEF, which we predicted to negatively correlate with alpha power, and two components of the CON in the pFC, encompassing the dorsal ACC (dACC) and the anterior pFC, for which we predicted the opposite relationship based on observed dissociations between these networks (Sadaghiani et al., 2010). Again, one-tailed tests were used based on these directional predictions.

Cross-correlation Analyses

To identify the temporal relationship between modulatory frontal brain areas and pretarget levels of alpha power, we conducted a seeded, backward-lagged cross-correlation using the envelope of the EROS alpha difference for detected and undetected targets in the cuneus as a common seed (shown in Figure 5C). This common seed was cross-correlated with the time course of the broadband, time domain-averaged EROS signal difference between detected and undetected targets in all other voxels. Correlating the seed with the broadband EROS signal allows us to identify correlates of cuneus alpha activity in areas that do not necessarily oscillate at 8–12 Hz themselves. In other words, it should allow us to identify whether any event-related preparatory activity predicts later alpha power differences.

Importantly, we only used 30 time points comprising the 847-msec data segment before target onset. Although this does include the evoked activity from the warning stimulus, we felt that this was important to identify any relationship between alpha modulations and preceding preparatory neural activity. Only evoked activity that correlated with subsequent alpha modulations will be revealed by this analysis.

The resultant correlations were then Fisher r-to-z transformed to remove the correlation's restricted range. On the basis of the Fisher-transformed individual participant's correlations, t statistics were then computed across participants and transformed into z scores for plotting and statistical tests in each ROI. This analysis was then repeated by shifting the target location time series negatively one sampling point compared with the seed's time series, creating what is essentially one half of a cross-correlation function for each voxel. To visualize the temporal progression, we then plotted this function at each of nine time lags instead of just locating the peak lag in each region. Correction for multiple comparisons was based on the same random field theory techniques described above, but each time-shifted analysis was conducted independently. We used this relatively liberal statistical threshold in this exploratory analysis to maximize our chance of uncovering possible candidate regions that correlate with subsequent alpha and better understand their temporal progression. This analysis tests not only for the instantaneous correlations with preparatory alpha but also whether differences in activity in one region early in the pretarget period, including activity evoked by the fixation cross, predict the difference in 10-Hz alpha activity in the cuneus later in the pretarget period. We tested for significant correlations between the difference in EROS alpha

cuneus activity and the difference in activity in each of the ROIs independently.

RESULTS

Behavioral Results

Unmasked targets were easily detected (M = 98.4%, SD = 2.0%, range = 93.2–100%), whereas participants detected masked targets only 63.8% of the time (SD = 19.1%, range = 29.2–90.7%), verifying the effectiveness of the metacontrast mask (M_{diff} = 34.6%; $t(15) = 7.76$, $p < .05$). In comparison, false alarms, in which participants indicated that a target was present when only a mask was shown, were rare (false alarm rate: M = 9.5%, SD = 8.1%, range = 0.3–25.1% of no-target trials). To estimate the ability of participants to differentiate the masked target from noise, we combined these measures and computed a d' for each participant (M = 1.91, SD = 0.60, range = 0.75–2.98). Although metacontrast masking was effective, as desired all participants still exhibited some sensitivity to the target (i.e., had values of d' greater than 0) due primarily to the longer target-to-mask SOA that we chose by design. Importantly, the balance between hits and misses, combined with the large number of trials, allowed us to separately measure brain activity for detected and undetected targets for each participant. The low level of false alarms precluded any analysis of brain activity preceding erroneous reports of target detection. The target-only trials were also not considered further because detection rates for these trials were nearly perfect. All further analyses were conducted only on the detected and undetected masked trials.

EEG Results

EEG Alpha Power

First we sought to replicate the findings of Mathewson and colleagues (2009) showing decreased alpha power preceding subsequently detected targets. Figure 3 shows the difference in EEG power between detected and undetected targets for the average of electrodes O1 and O2. Consistent with our previous results, the average power difference in the 8–12 Hz (alpha) band in the interval between the onset of the fixation and the onset of the target was significantly lower before subsequently detected targets ($M = -0.98\ \mu V^2$) than undetected targets ($M = -0.69\ \mu V^2$; $t(15) = 3.31$, $p < .05$). Note that this represents a greater decrease in alpha after the warning stimulus and before detected targets. We confirmed that alpha power was largest at these posterior electrodes. As can be seen in Figure 3, this alpha difference was maximal from 200 to 400 msec before the onset of the target. Note that data from any times after 200 msec pretarget would be contaminated from posttarget-evoked activity in the FFT window.

EROS Results

EROS Alpha Power

To localize pretarget modulated alpha oscillations concomitant with the observed EEG alpha difference, we next considered the coherent oscillatory alpha activity present in the EROS data. We predicted decreased alpha power compared with baseline in areas of DAN before detected compared with undetected targets. This difference in

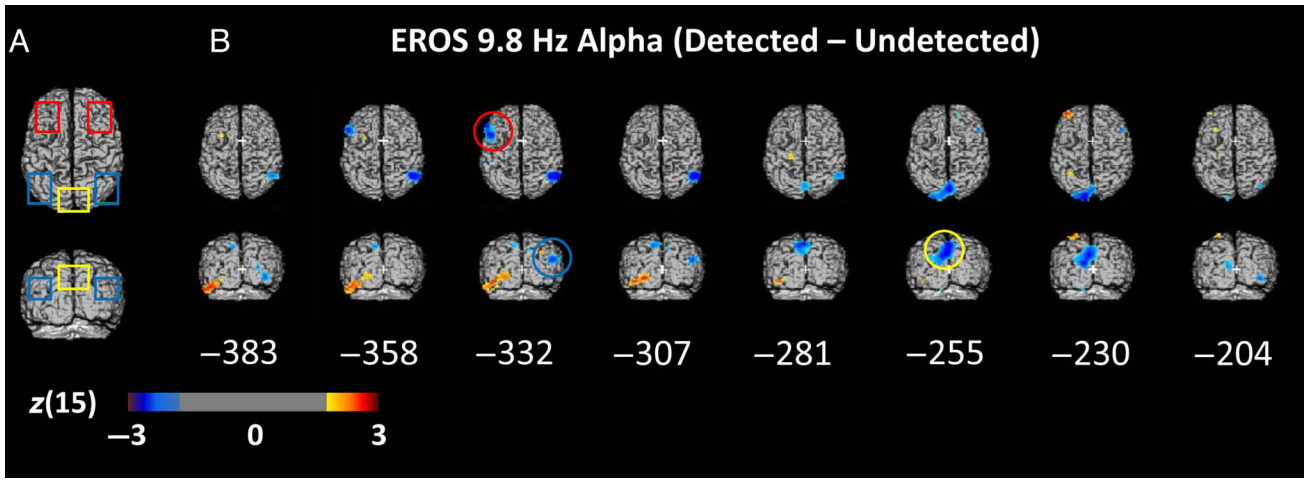

Figure 4. EROS Alpha. (A) Two-dimensional projections of bilateral frontal (red), bilateral inferior parietal (blue), and cuneus (yellow) ROIs. (B) Statistical parametric maps of the z-score difference between detected and undetected targets (detected − undetected) in 9.8 Hz phase-locked EROS alpha power for each 25.6-msec interval of the 400–200 msec before the onset of the masked target. The difference in phase-locked EROS alpha is shown projected orthogonally onto a common template of the superior axial (top) and posterior coronal (bottom) surfaces of a brain in Talairach space. Only z scores greater than 2 or less than −2 are plotted for visualization purposes representing a one-sided threshold of $\alpha \leq .0275$, uncorrected for multiple comparisons. Colored circles represent the time and location at which a significant difference in phase-locked EROS alpha power peaked in the color-corresponding ROI shown in A, corrected within each ROI for multiple comparisons with random field theory. Each time point and ROI were tested independently.

alpha EROS activity for the 400–200 msec period before target onset is shown in Figure 4B using two orthogonal projections (axial and coronal), uncorrected for multiple comparisons to visualize the temporal and spatial extent of the differences before ROI analysis. Colored circles indicate the peaks of significant differences in alpha activity between detected and undetected targets in the corresponding DAN ROI projections from Figure 4A and Table 2, corrected for multiple comparisons using random field theory.

There was an early decrease in EROS alpha activity before detected targets in left superior frontal regions peaking at 332 msec pretarget (left superior frontal gyrus [SFG]/middle frontal gyrus [MFG] ROI; peak $t(15) = -3.75$; $z(15) = -2.89$; $z_{crit} = -2.75$; peak coordinates: −51/12/38) and in the right inferior parietal areas also peaking at 332 msec before the target (right TPJ/IPS ROI; peak $t(15) = -3.72$; $z(15) = -2.87$; $z_{crit} = -2.56$; peak coordinates: −49/−72/19). These differences occurred before the onset of a large and sustained alpha difference in the cuneus and dorsal extrastriate regions from 281 to 230 msec before the target (cuneus/precuneus ROI; peak $t(15) = -4.35$; $z(15) = -3.25$; $z_{crit} = -2.71$; peak time: 255 msec; peak coordinates: −3/−71/42). Interestingly, there was an area of the left inferior temporal lobe (ITL) shown in Figure 4B that appeared to have higher alpha power before detected targets. This positive relationship between alpha power and detection in the ITL is consistent with findings from intracranial EEG in humans (Bollimunta, Mo, Schroeder, & Ding, 2011; Mo, Schroeder, & Ding, 2011), suggesting that alpha oscillations serve a different function in ITL than elsewhere in visual cortex.

Crucially, the maximal difference in 9.8 Hz EROS alpha power between detected and undetected targets in the

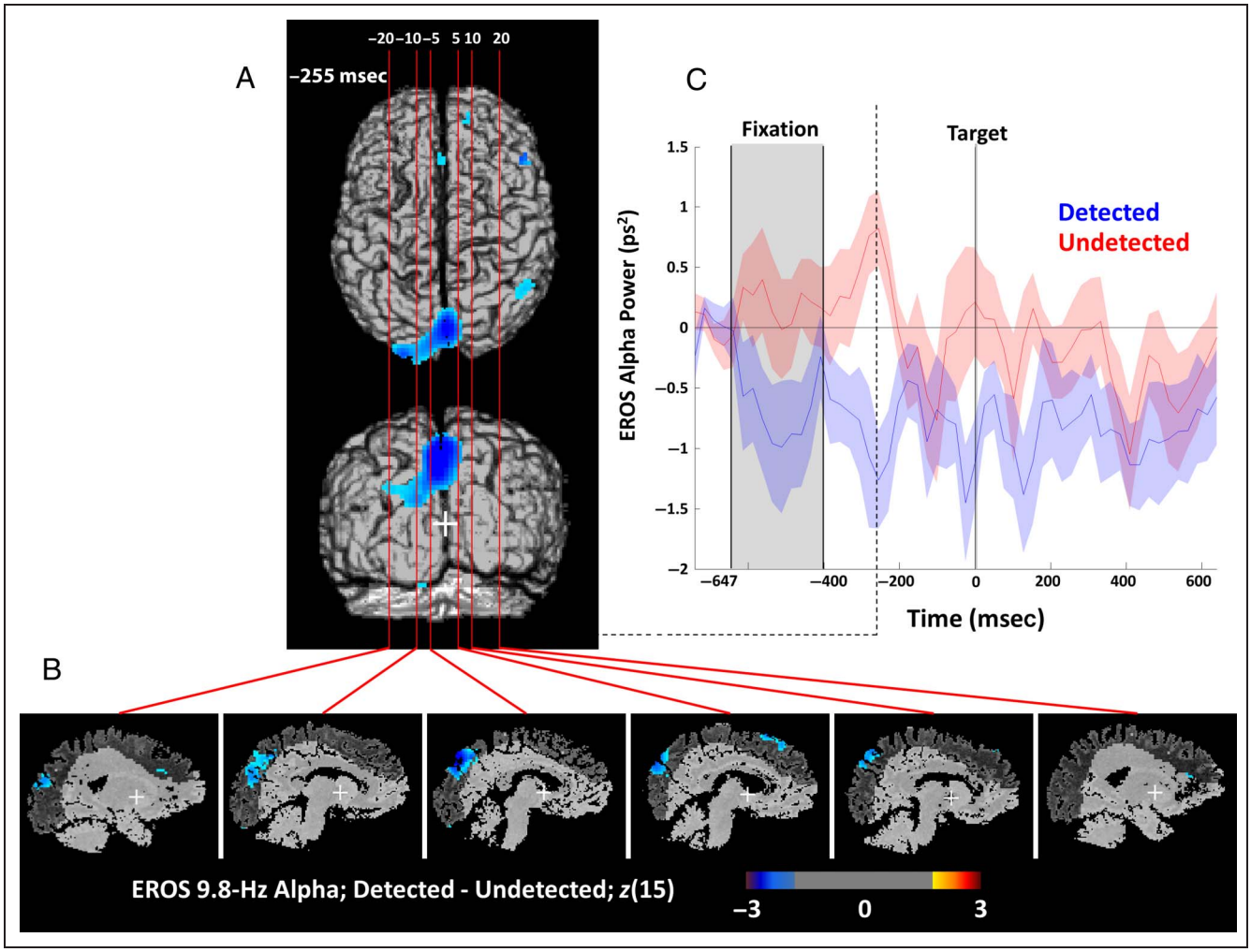

Figure 5. Phase-locked EROS alpha cuneus difference. (A) Surface projections of the difference between detected and undetected targets in 9.8-Hz EROS alpha power from Figure 4 are shown from two orthogonal angles, only for the time period in which the difference in alpha was largest in the cuneus ROI. Vertical lines indicate the six Talairach *x* planes from which the sagittal sections were taken. (B) Sagittal slices through the template brain with the difference in phase-locked EROS alpha power, indicating the horizontal extent and depth of the differences in oscillatory activity with a greater than 2 or less than −2 *z*-score threshold. Dark gray areas indicate cortical regions interrogated by the optical sources for at least four participants, showing widespread and deep coverage of parietal and frontal areas. (C) Trial time course of grand-averaged coherent alpha power of the spatially smoothed voxel with the peak cuneus difference in alpha between detected (blue) and undetected (red) trials from the posterior coronal projection. Shaded error bars represent ±1 *SEM*, and the dashed line shows the time of peak difference shown in A.

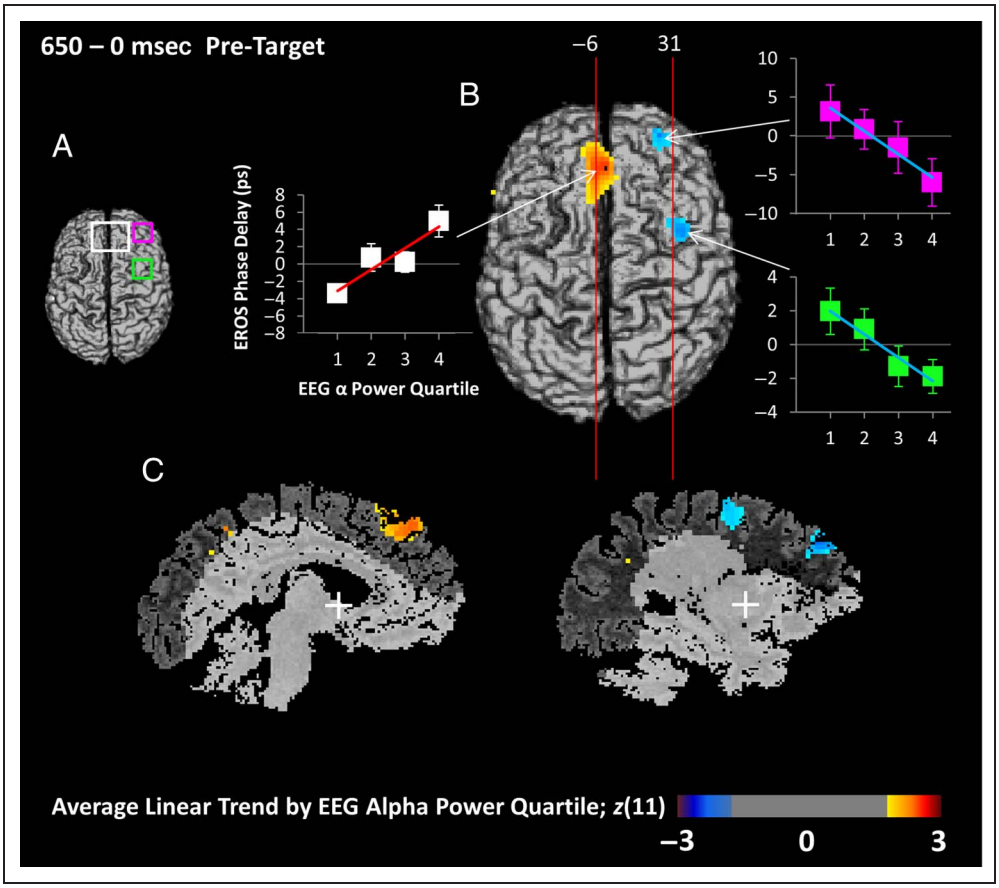

Figure 6. EROS sorted by EEG alpha. (A) Projections of the three ROIs used for analysis of these differences; dACC and medial pFC of the CON (white), right anterior pFC of the CON (pink), and right FEFs of the DAN (FEF; green). (B) Surface axial map depicting the relationship between EROS activity (averaged across the whole 650-msec pretarget period) and 8–12 Hz EEG alpha power. To obtain these data, single-trial EROS data were averaged into four bins based on EEG alpha power, and a linear trend analysis was conducted on the EROS bins, separately for each voxel. The EROS bin averages combined across participants at the peak location for each ROI are shown in the adjacent graphs, with error bars representing the *SEM*, and the line representing the linear trend across EEG alpha quartiles. The line's hue and slope are commensurate with the hue and intensity of that pixel in the brain image. Significance of this analysis is expressed as a z score correcting the t value for voxel level differences in degrees of freedom and used for constructing the maps which have a greater than 2 or less than −2 z-score uncorrected threshold. Red areas indicate an increase of EROS activity as 8–12 Hz EEG alpha power increases, whereas blue areas indicate the opposite. Vertical lines represent the planes from which the sagittal slices in C were taken. (C) Representative slices through the areas of significant difference at the two planes shown in B, indicating the spatial extent of the effects.

cuneus, 255 msec before the target, was positively correlated across participants with the difference in 8–12 Hz EEG alpha power (average of O1 and O2) measured during the pretarget window shown in Figure 3 (r = .47; $t(14)$ = 2.02; directional $p < .05$). Furthermore, the peak EROS alpha difference in the left SFG, 322 msec before the target was also positively correlated with the difference in EEG alpha power (r = .52, $t(14)$ = 2.28, $p < .05$). Interestingly, the EROS activity in the cuneus and SFG accounted for unique variance in EEG alpha, as they were not themselves strongly correlated (r = .20, *ns*). In contrast, the difference in the EROS alpha power in right inferior parietal cortex, which peaked at 332 msec, was weakly and negatively correlated with the detection-related difference in EEG alpha power (r = −.16, *ns*). Given the magnitude and location of the large cuneus/precuneus EROS difference in alpha, we identified it for further inquiry as a likely correlate of EEG alpha. The late timing of this difference in the cuneus adds further support to its relevance, as activity near the end of the preparatory period should be most relevant for subsequent target detection. Furthermore, this area is very similar to previously reported areas that negatively correlate with alpha power (e.g., Sadaghiani et al., 2010; but see Thut et al., 2011, for more anterior alpha localization in a spatial attention task).

Figure 5 shows the spatial distribution of alpha power differences at the temporal peak of the effect, 255 msec before target onset (Figure 5A and B), and the time course for detected and undetected targets at the peak voxel in the cuneus/precuneus ROI (Figure 5C). These data support the correspondence between the EEG and EROS measures of alpha activity and indicate that the cuneus is a likely source of the scalp-measured differences in EEG alpha related to visual awareness.

EROS Activity Associated with Increases in EEG Alpha Power

We next examined areas whose activity, although not oscillating at 8–12 Hz, was still associated with the modulation of alpha activity related to target detection. To this end, we measured single-trial EEG alpha power from 400 to 200 msec before the target (the window of maximal alpha difference) and sorted EROS trials into four bins of EEG alpha power. We then averaged the broadband (0.1–15 Hz) EROS data for each of these EEG power bins and

multiplied the averages by the respective weights (−1.5, −0.5, 0.5, 1.5) describing a linear trend based on EEG alpha power quartiles. Summed, weighted averages were compared across participants with a t test at each voxel against zero. This approach allowed us to identify those voxels within the brain (or specified ROIs; Figure 6A) where sustained neural activity is associated with EEG measures of alpha power. Because of the DAN and CON's differing roles in attention control, we expected opposite relationships with alpha power for the DAN and CON frontal ROIs.

The results of this trend analysis are presented in Figure 6B, which shows the three areas whose EROS activity was positively (red) or negatively (blue) associated across trials with the EEG alpha power quartiles. For the peak in each ROI, the mean EROS activity for each EEG alpha power bin is shown in a corresponding graph. The slope of the line in each graph is commensurate with the activation intensity shown in the brain image for that pixel. These three areas correspond to components of the DAN and CON, which have previously been shown to correlate with EEG alpha modulation (Sadaghiani et al., 2010, 2012; He et al., 2007). The higher the EEG alpha power quartile, the greater the mean EROS activity in dorsal ACC (dACC; CON; ROI peak $t(11) = 3.24$; $z(11) = 2.80$; $z_{crit} = 2.57$; peak coordinates: −3/34/34).

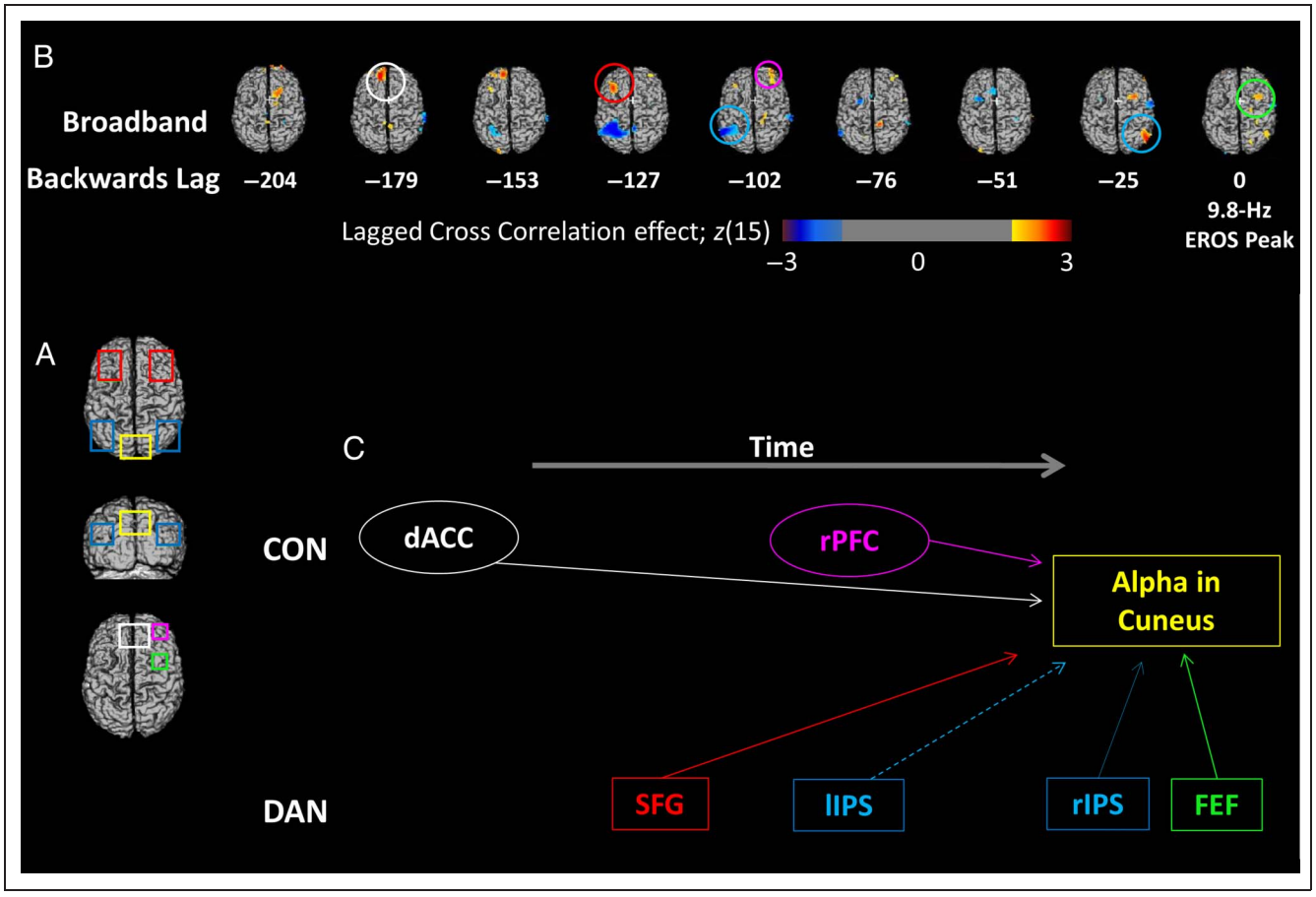

Figure 7. Cross-correlations. (A) The ROIs used for cross-correlation analyses. (B) The results of a lagged cross-correlation analysis using as a seed the time course of EROS alpha power at the point in the cuneus (see from Figure 5) where this power maximally differentiates undetected and detected targets. This activity is cross-correlated (with varying negative lags) with the time course of the time domain broadband EROS signal (also obtained by subtracting the undetected from the detected condition) for each voxel. The cross-correlations obtained from each participant are then Fisher-transformed and subjected to statistical parametric analysis across participants testing their difference from zero. The z scores associated with this parametric analysis are used to construct the maps. The data from lag 0 are shown on the right. To the left of this, time courses shifted at each lag from −204 to −25 msec are shown, revealing areas of the brain that predict subsequent suppression in 9.8-Hz EROS alpha activity in the cuneus on detected versus undetected trials. Red colors indicate areas where EROS alpha differences correlate positively with subsequent or concurrent cuneus alpha suppression, whereas blue areas represent activity that correlates negatively with alpha suppression. Colored circles represent the area and time point of maximal correlation in each of the given ROIs shown in A. (C) Temporal progression of the correlations between each of the ROIs and the suppression in posterior alpha oscillations, considering the lags at which EROS activity for each ROI was maximally correlated with subsequent alpha modulations. Solid lines indicate areas that showed positive correlations with alpha power suppression at Lag 0 and thus may directly communicate with cuneus areas, whereas dashed lines show negative relationships. The hypothetical flow of information over time is shown progressing from left to right. The DAN areas are shown separately from the CON areas, revealing the different temporal relationships of these regions with cuneus alpha suppression.

Conversely, as predicted, mean EROS activity was negatively associated with EEG alpha power in a region of the DAN, the right FEF (ROI peak $t(11) = -3.26$; $z(11) = -2.43$; $z_{crit} = -2.18$; peak coordinates: 39/−1/45), but also in another CON region, the right anterior pFC (ROI peak $t(11) = -3.33$; $z(11) = -2.47$; $z_{crit} = -2.35$; peak coordinates: 27/49/26). Two representative sagittal slices crossing the clusters of activation reveal the depth of the areas showing associations between mean EROS activity and EEG alpha (Figure 6C). Following Sadaghiani and colleagues (2012), we suggest that activity in dACC (a component of CON) maintains sustained tonic levels of alpha for the task, whereas the activity in the FEF (a DAN region) implements more dynamic and phasic adjustments based on the predictability of the upcoming stimulus.

Cross-correlation Analyses of EROS Data

To understand the temporal interplay between the modulatory frontoparietal areas and the prestimulus suppression of posterior alpha oscillations, we computed negative-lagged cross-correlations using 768 msec of data from the location of maximal EROS alpha difference between detected and undetected targets in the cuneus as a seed (see Figure 5). This analysis provides information about the relative timing of relationships between alpha suppression in sensory cortex and activity in the frontal modulatory areas identified in the preceding analyses. To investigate the network of brain areas whose activity at other frequencies was related to the modulation of alpha activity, we correlated the differences in activity from the cuneus seed region with time domain broadband (0.1–15 Hz) differences in EROS activity (Figure 7C). This exploratory analysis identifies the time lags of associations between sensory alpha and modulatory areas whose activity does not necessarily oscillate coherently in the alpha frequency range. We used relatively liberal statistical thresholds uncorrected for multiple comparisons because we were interested in the peak time and direction and not the significance per se. There were positive correlations with the cuneus alpha activity from −25 to 0 msec in both the right FEF (peak $t(15) = 3.12$; $z(15) = 2.84$; $z_{crit} = 2.27$; peak lag: 25 msec; peak coordinates: 32/9/51) and in the right inferior parietal lobe (peak $t(15) = 3.01$; $z(15) = 3.20$; $z_{crit} = 2.76$; peak lag: 25 msec; peak coordinates: 54/−78/85). Earlier in time, there was a negative correlation from −127 to −76 msec in the left superior parietal ROI (peak $t(15) = -4.42$; $z(15) = -3.29$; $z_{crit} = -2.58$; peak lag: 102 msec; peak coordinates: −33/−58/51), a positive correlation in right anterior prefrontal areas (peak $t(15) = 2.63$; $z(15) = 2.47$; $z_{crit} = 2.44$; peak lag: 102 msec; 34/47/27), and a positive correlation in left frontal areas (peak $t(15) = 3.23$; $z(15) = 2.92$; $z_{crit} = 2.77$; peak lag: 127 msec; peak coordinates: −36/27/38). Finally there was a positive correlation between EROS alpha band activity in the cuneus and the broadband time domain EROS activity in the dACC at −179 and −153 msec (peak $t(15) = 3.87$; $z(15) = 3.34$; $z_{crit} = 2.82$; 179 msec; −13/47/35).

A summary of the temporal progression of this modulatory activity is presented in Figure 7C, with the color of the box and text corresponding to the ROIs shown in Figure 7A. Note that the peak correlation for the DAN areas was closer in time to the maximal alpha suppression in the cuneus than it was for the dACC CON area, supporting the proposed complementary roles for these two networks. More specifically, the data are consistent with the idea that CON's role is to sustain tonic alpha/alertness and DAN's role is to temporarily shift alpha/attention based on task demands. Together, these cross-correlations provide further evidence that the DAN and CON have complementary modulatory influences on posterior alpha oscillations (see Sadaghiani et al., 2010), which, in turn, predict subsequent awareness.

DISCUSSION

We used fast optical imaging (EROS) of the human cortex combined with simultaneous EEG to localize the cortical sources of alpha oscillations that influence subsequent visual awareness and their possible control sites in the DAN and CON. Alpha suppression preceding the onset of sensory stimuli predicts subsequent processing and detection (Van Dijk, Van Der Werf, Mazaheri, Medendorp, & Jensen, 2010; Mathewson et al., 2009; Romei et al., 2008; Hanslmayr et al., 2007). Here we replicated this result, finding that EEG alpha power differed between detected and undetected masked visual targets with a peak difference around 300 msec pretarget.

We looked for a similar effect in the oscillatory EROS alpha activity by computing a time–frequency transform of the stimulus-related averaged EROS data and reconstructing the time course of coherent EROS alpha power that discriminated between detected and undetected targets. The strongest effect was observed in the cuneus and dorsal extrastriate visual areas around 255 msec before the onset of the target. This difference was widespread and robust, and lasted for approximately 100 msec, consistent with the time course of the alpha effect in the EEG data (Figure 5C). The difference in EEG alpha was correlated across participants with the difference in EROS alpha in this area. There was also a smaller correlation between the EEG and the EROS alpha difference in the left SFG earlier on before the target. However, given the timing relative to target onset, location, and magnitude of the EROS alpha suppression, the cuneus is the most likely source of the detection-related posterior EEG alpha suppression with which it is correlated. Other investigators have previously modeled the sources of alpha oscillations important for visual awareness on the basis of MEG or EEG data. The source of discrimination-related differences in MEG alpha was estimated to be at a location along the parieto-occipital sulcus, close to the area of maximal

EROS alpha difference in the cuneus reported in Figure 5 (Van Dijk et al., 2010). Thut and colleagues (2011) used MEG to localize the modulations in alpha in a spatial attention task to a slightly more anterior area of the cortex under electrode CP4. This anterior to posterior difference in alpha generation may represent different alpha generators for sustained compared with temporally directed attention.

EROS alpha power was also lower before detected than undetected targets in a number of other areas in frontoparietal cortex. This included the left SFG and the right inferior parietal lobule, approximately 350 msec before target onset. The inferior parietal lobule has been recently implicated as part of another frontoparietal network often referred to as the ventral attention network (VAN), which is associated with increased long-range alpha phase synchrony during resting states (Sadaghiani et al., 2012).

Much of the extant research on localization of alpha oscillations aims to correlate the EEG power envelope with resting hemodynamic activity, which is too temporally sluggish to detect alpha oscillations with high spatial precision. To provide a novel comparison with hemodynamic correlations, we binned the EROS data as a function of the simultaneously measured posterior EEG alpha power, irrespective of the subsequent behavioral outcome, and averaged the resultant contrast over the entire prestimulus period. This analysis provides a measure of the sustained modulatory influence, which may not necessarily be oscillating at the same frequency, on alpha oscillations before stimulus onset. We found two areas in the right pFC whose variations in activity were negatively associated with variations in EEG alpha power, one of them notably in the FEF. The FEF, a part of the DAN, has been implicated in top–down modulation of attention (He et al., 2007; Moore & Armstrong, 2003; Corbetta & Shulman, 2002). The observed relationship thus provides evidence for the involvement of the DAN in posterior alpha modulation (Sadaghiani et al., 2010; Moosmann et al., 2003; Laufs et al., 2002). Previous studies combining EEG with fMRI have also found large negative correlations between posterior alpha and hemodynamic activity in other DAN areas around the intraparietal sulcus (Sadaghiani et al., 2010; Babiloni et al., 2005), inferior parietal lobule (Moosmann et al., 2003; Laufs et al., 2002), and the superior parietal lobule (Sadaghiani et al., 2010; Laufs et al., 2002), as well as other frontal areas (Moosmann et al., 2003; Laufs et al., 2002) and in dorsal and lingual extrastriate visual areas (Sadaghiani et al., 2010; Moosmann et al., 2003). Positive correlations between EEG alpha power and hemodynamic activity in the CON have been reported, including areas of the thalamus (Goldman, Stern, Engel, & Cohen, 2002), insula, and dACC (Sadaghiani et al., 2010; Laufs et al., 2002). Because of their depth, we were unable to measure activity from the thalamus or insula, which are considered to be important modulators of sensory alpha activity (e.g., Lopes Da Silva, 1991). Combining EROS, EEG, and fMRI (e.g., Gratton et al., 1997) will be useful to illuminate the relationship between our results and modulatory thalamic activity.

We found a large area over medial pFC and dACC where variations in activity were positively associated with variations in alpha suppression. The dACC is a component of the CON, which Sadaghiani and colleagues (2010) found to correlate positively with resting alpha power. The more ventral parts of this activation in the medial prefrontal area, along with the ventral cuneus where the largest EROS alpha modulation was observed, have been implicated as part of the network of brain areas more active during resting or task-irrelevant processing (Buckner, Andrews-Hanna, & Schacter, 2008; Dosenbach et al., 2007), supporting previous findings of the relationship between alpha oscillations and activity of DMN (e.g., Mo et al., 2012; Ben-Simon et al., 2008). Activity in DMN and CON before the onset of the target predicts subsequent lapses in awareness. This finding opens up the possibility of monitoring in real time the vigilance state of the individual, based on optical measures of activation in the medial prefrontal and cuneus areas, as well as EEG and EROS alpha oscillations.

We also tested the extent to which these modulatory areas form networks to control alpha oscillations. The EROS alpha difference in the cuneus was used as a seed for cross-correlation with all other areas, both coincident in time and at various negative lags, such that activity was highlighted that predicted subsequent alpha suppression. We found a progression of correlated areas in the DAN that predicted subsequent alpha range suppression in the cuneus. Almost all DAN ROIs revealed positive correlations with subsequent posterior alpha suppression occurring approximately 150 msec later. Earlier in time, a correlation was found with dACC (a CON region) at an interval of approximately 180 msec before the alpha suppression. This backward progression reveals the dynamics of the network of brain areas modulating the subsequent alpha power differences in sensory cortices. This progression supports the proposed complementary roles for the CON and DAN in alpha modulation as that of a tonic "maintainer" and a dynamic selective "attender," respectively (Sadaghiani et al., 2010). Recently, Sadaghiani and colleagues (2012), using simultaneous fMRI and EEG, have shown that hemodynamic activity in another frontoparietal network, the VAN, is associated with long-range alpha phase synchrony, which has been proposed to implement the adaptive changes in modulation of sensory areas based on exogenous and endogenous attentional reorientation (e.g., Palva & Palva, 2011). Our results are consistent with this proposed role for long-range synchrony, but here in the service of detecting a near-threshold target. In future research, we plan to probe these VAN areas with single-pulse TMS during the time intervals highlighted in the current study to test whether they play a causal role in posterior alpha and detection.

In summary, with the novel exploratory power afforded by a combination of large-scale fast optical imaging with

EROS and concurrent EEG recordings, we found a relationship between top–down modulations from frontoparietal attention networks, fluctuations in oscillatory alpha activity in sensory areas, and subsequent visual awareness. We measured the power of alpha oscillations in the EROS data with high spatial and temporal resolution and identified a large area in the cuneus where alpha oscillations differed between detected and undetected targets. Across three separate analyses, we also identified modulators of this posterior alpha activity in areas of the DAN and CON, where EROS activity was associated with preparatory EEG power. Finally, taking advantage of the high temporal resolution of EROS, we found that activity in the DAN and CON preceded and was correlated with subsequent preparatory alpha suppression in the cuneus. These findings support the predictions of our pulsed-inhibition account of alpha oscillations (Mathewson et al., 2009, 2011, 2012) in which top–down preparation from DAN is proposed to modulate the sensory-relevant inhibitory alpha activity using phasic pulses of inhibition.

Acknowledgments

The work was supported by a Natural Science and Engineering Research Council of Canada fellowship and a Beckman postdoctoral fellowship to K. E. M. as well as NIMH R56MH097973 grant to G. G. The authors would like to thank Tanya Stanley, Jamie Jones, and Chris Prudhomme for assistance with data collection.

Reprint requests should be sent to Kyle E. Mathewson, Beckman Institute, 405 N. Mathews Ave., Urbana, IL 61801, or via e-mail: kmathew3@illinois.edu.

REFERENCES

Andrew, R. D., & MacVicar, B. A. (1994). Imaging cell volume changes and neuronal excitation in the hippocampal slice. *Neuroscience, 62,* 371–383.

Babiloni, F., Cincotti, F., Babiloni, C., Carducci, F., Mattia, D., Astolfi, L., et al. (2005). Estimation of the cortical functional connectivity with the multimodal integration of high-resolution EEG and fMRI data by directed transfer function. *Neuroimage, 24,* 118–131.

Ben-Simon, E., Podlipsky, I., Arieli, A., Zhdanov, A., & Hendler, T. (2008). Never resting brain: Simultaneous representation of two alpha related processes in humans. *PloS One, 3,* e3984.

Berger, H. (1929). Über das Elektroenkephalogramm des Menschen. *Archiv fur Psychiatrie und Nervenkrankheiten, 87,* 527–570.

Bollimunta, A., Mo, J., Schroeder, C. E., & Ding, M. (2011). Neuronal mechanisms and attentional modulation of corticothalamic alpha oscillations. *Journal of Neuroscience, 31,* 4935–4943.

Buckner, R. L., Andrews-Hanna, J. R., & Schacter, D. L. (2008). The brain's default network. *Annals of the New York Academy of Sciences, 1124,* 1–38.

Capotosto, P., Babiloni, C., Romani, G. L., & Corbetta, M. (2012). Differential contribution of right and left parietal cortex to the control of spatial attention: A simultaneous EEG-rTMS study. *Cerebral Cortex, 22,* 446–454.

Chiarelli, A. M., DiVacri, A., Romani, G. L., & Merla, A. (2012). Fast optical signal in visual cortex: Improving detection by General Linear Convolution Model. *Neuroimage, 66,* 194–202.

Corbetta, M., & Shulman, G. L. (2002). Control of goal-directed and stimulus-driven attention in the brain. *Nature Reviews Neuroscience, 3,* 215–229.

Dosenbach, N. U., Fair, D. A., Miezin, F. M., Cohen, A. L., Wenger, K. K., Dosenbach, R. A., et al. (2007). Distinct brain networks for adaptive and stable task control in humans. *Proceedings of the National Academy of Sciences, U.S.A., 104,* 11073–11078.

Fabiani, M., Gordon, B. A., Maclin, E. L., Pearson, M., Brumback, C. R., Low, K. A., et al. (2014). Neurovascular coupling in normal aging: A combined optical, ERP and fMRI study. *Neuroimage, 1,* 592–607.

Franceschini, M. A., & Boas, D. A. (2004). Noninvasive measurement of neuronal activity with near-infrared optical imaging. *Neuroimage, 21,* 372–386.

Frostig, R. D., & Chen-Bee, C. H. (2009). Visualizing adult cortical plasticity using intrinsic signal optical imaging. *In Vivo Optical Imaging of Brain Function, 2,* 255–287.

Goldman, R. I., Stern, J. M., Engel, J., Jr., & Cohen, M. S. (2002). Simultaneous EEG and fMRI of the alpha rhythm. *NeuroReport, 13,* 2487.

Gratton, G., Coles, M. G., & Donchin, E. (1983). A new method for off-line removal of ocular artifact. *Electroencephalography and Clinical Neurophysiology, 55,* 468–484.

Gratton, G., & Corballis, P. M. (1995). Removing the heart from the brain: Compensation for the pulse artifact in the photon migration signal. *Psychophysiology, 32,* 292–299.

Gratton, G., & Fabiani, M. (2003). The event related optical signal (EROS) in visual cortex: Replicability, consistency, localization and resolution. *Psychophysiology, 40,* 561–571.

Gratton, G., & Fabiani, M. (2010). Fast optical imaging of human brain function. *Frontiers in Human Neuroscience, 4,* 9.

Gratton, G., Fabiani, M., Corballis, P. M., Hood, D. C., Goodman-Wood, M. R., Hirsch, J., et al. (1997). Fast and localized event-related optical signals (EROS) in the human occipital cortex: Comparison with the visual evoked potential and fMRI. *Neuroimage, 6,* 168–180.

Gratton, G., Goodman-Wood, M. R., & Fabiani, M. (2001). Comparison of neuronal and hemodynamic measure of the brain response to visual stimulation: An optical imaging study. *Human Brain Mapping, 13,* 13–25.

Gratton, G., Sarno, A. J., Maclin, E., Corballis, P. M., & Fabiani, M. (2000). Toward noninvasive 3-D imaging of the time course of cortical activity: Investigation of the depth of the event-related optical signal (EROS). *Neuroimage, 11,* 491–504.

Hamidi, M., Slagter, H. A., Tononi, G., & Postle, B. R. (2009). Repetitive transcranial magnetic stimulation affects behavior by biasing endogenous cortical oscillations. *Frontiers in Integrative Neuroscience, 3,* 1–12.

Hanslmayr, S., Aslan, A., Staudigl, T., Klimesch, W., Herrmann, C. S., & Bäuml, K.-H. (2007). Prestimulus oscillations predict visual perception performance between and within subjects. *Neuroimage, 37,* 1465–1473.

He, B. J., Snyder, A. Z., Vincent, J. L., Epstein, A., Shulman, G. L., & Corbetta, M. (2007). Breakdown of functional connectivity in frontoparietal networks underlies behavioral deficits in spatial neglect. *Neuron, 53,* 905–918.

Huang, J., Wang, S., Jia, S., Mo, D., & Chen, H. C. (2013). Cortical dynamics of semantic processing during sentence comprehension: Evidence from event-related optical signals. *PloS One, 8,* e70671.

Jensen, O., & Mazaheri, A. (2010). Shaping functional architecture by oscillatory alpha activity: Gating by inhibition. *Frontiers in Human Neuroscience, 4*.
Kiebel, S. J., Poline, J. B., Friston, K. J., Holmes, A. P., & Worsley, K. J. (1999). Robust smoothness estimation in statistical parametric maps using standardized residuals from the general linear model. *Neuroimage, 10,* 756–766.
Klimesch, W. (1999). EEG alpha and theta oscillations reflect cognitive and memory performance: A review and analysis. *Brain Research Reviews, 29,* 169–195.
Klimesch, W., Sauseng, P., & Hanslmayr, S. (2007). EEG alpha oscillations: The inhibition-timing hypothesis. *Brain Research Reviews, 53,* 63–88.
Laufs, H., Kleinschmidt, A., Beyerle, A., Eger, E., Salek-Haddadi, A., Preibisch, C., et al. (2003). EEG-correlated fMRI of human alpha activity. *Neuroimage, 19,* 1463–1476.
Lee, J., & Kim, S. J. (2010). Spectrum measurement of fast optical signal of neural activity in brain tissue and its theoretical origin. *Neuroimage, 51,* 713–722.
Lopes Da Silva, F. H. (1991). Neural mechanisms underlying brain waves: From neural membranes to networks. *Electroencephalography and Clinical Neurophysiology, 79,* 81–93.
Low, K. A., Leaver, E., Kramer, A. F., Fabiani, M., & Gratton, G. (2006). Fast optical imaging of frontal cortex during active and passive oddball tasks. *Psychophysiology, 43,* 127–136.
Low, K. A., Leaver, E., Kramer, A. F., Fabiani, M., & Gratton, G. (2009). Share or compete? Load-dependent recruitment of prefrontal cortex during dual-task performance. *Psychophysiology, 46,* 1–11.
Mathewson, K. E., Gratton, G., Fabiani, M., Beck, D. M., & Ro, T. (2009). To see or not to see: Prestimulus alpha phase predicts visual awareness. *Journal of Neuroscience, 29,* 2725–2732.
Mathewson, K. E., Lleras, A., Beck, D. M., Fabiani, M., Ro, T., & Gratton, G. (2011). Pulsed out of awareness: EEG alpha oscillations represent a pulsed-inhibition of ongoing cortical processing. *Frontiers in Psychology, 2*.
Mathewson, K. E., Prudhomme, C., Fabiani, M., Beck, D. M., Lleras, A., & Gratton, G. (2012). Making waves in the stream of consciousness: Entraining oscillations in EEG alpha and fluctuations in visual awareness with rhythmic visual stimulation. *Journal of Cognitive Neuroscience, 24,* 2321–2333.
Medvedev, A. V., Kainerstorfer, J., Borisov, S. V., Barbour, R. L., & VanMeter, J. (2008). Event-related fast optical signal in a rapid object recognition task: Improving detection by the independent component analysis. *Brain Research, 1236,* 145–158.
Medvedev, A. V., Kainerstorfer, J. M., Borisov, S. V., Gandjbakhche, A. H., & VanMeter, J. (2010). "Seeing" electroencephalogram through the skull: Imaging prefrontal cortex with fast optical signal. *Journal of Biomedical Optics, 15,* 061702–061702.
Mo, J., Liu, Y., Huang, H., & Ding, M. (2012). Coupling between visual alpha oscillations and default mode activity. *Neuroimage, 68,* 112–118.
Mo, J., Schroeder, C. E., & Ding, M. (2011). Attentional modulation of alpha oscillations in macaque inferotemporal cortex. *Journal of Neuroscience, 31,* 878–882.
Momose-Sato, Y., Sato, K., Hirota, A., & Kamino, K. (1998). GABA-induced intrinsic light-scattering changes associated with voltage-sensitive dye signals in embryonic brain stem slices: Coupling of depolarization and cell shrinkage. *Journal of Neurophysiology, 79,* 2208–2217.
Moore, T., & Armstrong, K. M. (2003). Selective gating of visual signals by microstimulation of frontal cortex. *Nature, 421,* 370–373.
Moosmann, M., Ritter, P., Krastel, I., Brink, A., Thees, S., Blankenburg, F., et al. (2003). Correlates of alpha rhythm in functional magnetic resonance imaging and near infrared spectroscopy. *Neuroimage, 20,* 145–158.
Palva, S., & Palva, J. M. (2011). Functional roles of alpha-band phase synchronization in local and large-scale cortical networks. *Frontiers in Psychology, 2*.
Rector, D. M., Carter, K. M., Volegov, P. L., & George, J. S. (2005). Spatio-temporal mapping of rat whisker barrels with fast scattered light signals. *Neuroimage, 26,* 619.
Rector, D. M., Poe, G. R., Kristensen, M. P., & Harper, R. M. (1997). Light scattering changes follow evoked potentials from hippocampal Schaeffer collateral stimulation. *Journal of Neurophysiology, 78,* 1707–1713.
Romei, V., Brodbeck, V., Michel, C., Amedi, A., Pascual-Leone, A., & Thut, G. (2008). Spontaneous fluctuations in posterior alpha-band EEG activity reflect variability in excitability of human visual areas. *Cerebral Cortex, 18,* 2010–2018.
Sadaghiani, S., Scheeringa, R., Lehongre, K., Morillon, B., Giraud, A. L., D'Esposito, M., et al. (2012). Alpha-band phase synchrony is related to activity in the frontoparietal adaptive control network. *Journal of Neuroscience, 32,* 14305–14310.
Sadaghiani, S., Scheeringa, R., Lehongre, K., Morillon, B., Giraud, A. L., & Kleinschmidt, A. (2010). Intrinsic connectivity networks, alpha oscillations, and tonic alertness: A simultaneous electroencephalography/functional magnetic resonance imaging study. *Journal of Neuroscience, 30,* 10243–10250.
Sato, K., Momose-Sato, Y., Arai, Y., Hirota, A., & Kamino, K. (1997). Optical illustration of glutamate-induced cell swelling coupled with membrane depolarization in embryonic brain stem slices. *NeuroReport, 8,* 3559.
Sun, B., Zhang, L., Gong, H., Sun, J., & Luo, Q. (2014). Detection of optical neuronal signals in the visual cortex using continuous wave near-infrared spectroscopy. *Neuroimage, 87,* 190–198.
Syková, E., Kubinová, S., Jendelová, P., & Chvátal, A. (2003). The relationship between changes in intrinsic optical signals and cell swelling in rat spinal cord slices. *Neuroimage, 18,* 214–230.
Thut, G., Veniero, D., Romei, V., Miniussi, C., Schyns, P., & Gross, J. (2011). Rhythmic TMS causes local entrainment of natural oscillatory signatures. *Current Biology, 21,* 1176–1185.
Tse, C. Y., Gordon, B. A., Fabiani, M., & Gratton, G. (2010). Frequency analysis of the visual steady-state response measured with the fast optical signal in younger and older adults. *Biological Psychology, 85,* 79–89.
Van Dijk, H., Van Der Werf, J., Mazaheri, A., Medendorp, W. P., & Jensen, O. (2010). Modulations in oscillatory activity with amplitude asymmetry can produce cognitively relevant event-related responses. *Proceedings of the National Academy of Science, 107,* 900–905.
Whalen, C., Maclin, E. L., Fabiani, M., & Gratton, G. (2008). Validation of a method for coregistering scalp recording locations with 3D structural MR images. *Human Brain Mapping, 29,* 1288–1301.
Witte, O. W., Niermann, H., & Holthoff, K. (2001). Cell swelling and ion redistribution assessed with intrinsic optical signals. *Anais da Academia Brasileira de Ciências, 73,* 337–350.
Worsley, K. J., & Friston, K. J. (1995). Analysis of fMRI time-series revisited—Again. *Neuroimage, 2,* 173–181.
Zhang, F., Wang, L. P., Brauner, M., Liewald, J. F., Kay, K., Watzke, N., et al. (2007). Multimodal fast optical interrogation of neural circuitry. *Nature, 446,* 633–639.